Research Article

Received: 22 June 2019 Revised: 10 August 2019 Accepted article published: 16 August 2019 Published online in Wiley Online Library: 10 September 2019

(wileyonlinelibrary.com) DOI 10.1002/pi.5909

3D printing hybrid organometallic polymer-based biomaterials via laser two-photon polymerization

Evaldas Balčiūnas,[a] Sara J Baldock,[b,c] Nadežda Dreižė,[a] Monika Grubliauskaitė,[a] Sarah Coultas,[d] David L Rochester,[b] Mindaugas Valius,[a] John G Hardy[b,c*] and Daiva Baltriukienė[a*]

Abstract

Materials with microscale structures are gaining increasing interest due to their range of technical and medical applications. Additive manufacturing approaches to such objects via laser two-photon polymerization, also known as multiphoton fabrication, enable the creation of new materials with diverse and tunable properties. Here, we investigate the properties of 3D structures composed of organometallic polymers incorporating aluminium, titanium, vanadium and zirconium. The organometallic polymer-based materials were analysed using a variety of techniques including SEM, energy-dispersive X-ray spectroscopy, X-ray photoelectron spectroscopy analysis and contact angle measurements and their biocompatibility was tested *in vitro*. Cell viability and mode of death were determined by 3-(4,5-dimethyl-2-thiazolyl)-2,5-diphenyl-2H-tetrazolium bromide (MTT) assay and acridine orange/ethidium bromide staining. Polymers incorporating Al, Ti and Zr supported cell adhesion and proliferation, and showed low toxicity *in vitro*, whereas the organometallic polymer incorporating V was shown to be cytotoxic. Inductively coupled plasma optical emission spectrometry suggested that leaching of the V from the organometallic polymer is the likely cause of this. The preparation of the organometallic polymers is straightforward and both simple 2D and complex 3D structures can be fabricated with ease. Resolution tests of the newly developed organometallic polymer incorporating Al show that suspended lines with widths down to 200 nm can be fabricated. We believe that the materials described in this work show promising properties for the development of objects with sub-micron features for biomedical applications (e.g. biosensors, drug delivery devices, tissue scaffolds etc.).

Supporting information may be found in the online version of this article.

Keywords: 3D printing; laser two-photon polymerization; photopolymers; organometallic polymers; tissue engineering

INTRODUCTION

Laser two-photon polymerization (LTPP) is a very promising technique for 3D microstructure fabrication. It has been used to make structures for a variety of applications, ranging from photonic crystals,[1] metamaterials,[2] micromachines,[3] waveguides,[4] microoptical components,[5] microelectromechanical systems[6] and scaffolds for tissue engineering.[7] Some excellent reviews regarding the use of LTPP for biological applications have been written.[8–10] Various materials can be polymerized using LTPP systems, including polyethylene glycol-diacrylate,[11] epoxy-based glycidyl ether of bisphenol A (SU-8),[12] gelatine methacrylate[13] and many others. The materials can incorporate drugs, quantum dots or even living cells. Gittard *et al.* have reported the fabrication of microneedles doped with gentamicin sulfate.[14] Jia *et al.* have fabricated quantum dot doped structures with nonlinear optical properties.[15] Marino *et al.* have functionalized commercially available Ormocomp® photopolymer with barium titanate nanoparticles, endowing it with piezoelectric properties.[16] Ovsianikov *et al.* have demonstrated the possibility of encapsulating living cells inside photopolymerizable materials and keeping them viable after structure formation.[17]

The chemical, mechanical and topographical properties of materials can influence cellular processes. It has been shown that cellular differentiation can be affected by matrix stiffness[18] or topography.[19] Cellular proliferation rate can be tuned by treating

* *Correspondence to: JG Hardy, Department of Chemistry, Lancaster University, Lancaster, UK, E-mail: j.g.hardy@lancaster.ac.uk; or D Baltriukienė, Institute of Biochemistry, Life Sciences Centre, Vilnius University, Vilnius, Lithuania. E-mail: daiva.baltriukiene@bchi.vu.lt*

a *Institute of Biochemistry, Life Sciences Centre, Vilnius University, Vilnius, Lithuania*

b *Department of Chemistry, Lancaster University, Lancaster, UK*

c *Materials Science Institute, Lancaster University, Lancaster, UK*

d *Kratos Analytical Ltd, Manchester, UK*

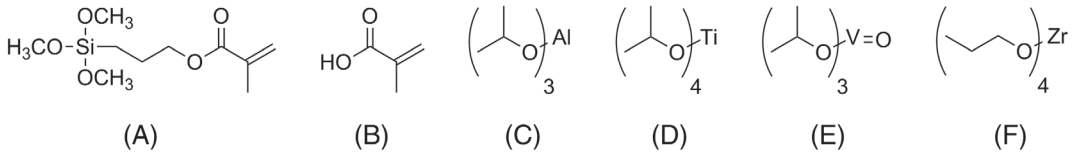

Figure 1. Components used in the organometallic polymers studied here: (A) 3-(trimethoxysilyl)propyl methacrylate; (B) methacrylic acid; (C) aluminium isopropoxide; (D) titanium(IV) isopropoxide; (E) vanadium(V) oxytriisopropoxide; (F) zirconium(IV) propoxide.

the substrate in various ways. Hamid *et al.* showed that modifying the chemical properties of materials by plasma treatment can significantly improve the biocompatibility of SU-8 microfluidic chips,[20] and a study by Thrivikraman *et al.* demonstrated the effects of electrical conductivity on cellular proliferation and differentiation.[21]

LTPP-fabricated structures have been investigated for their potential as scaffolds for tissue engineering applications.[7,22–24] 3D structures capable of supporting embryonic stem cells in an undifferentiated state without the use of feeder cells have been demonstrated before.[25]

A widely investigated class of materials for LTPP are hybrid organic–inorganic materials, some of which are based on organometallic polymers.[26] These materials are composed of metal alkoxides and acrylates that often contain silicon oxide. In most cases, the hybrid materials are rendered photosensitive by adding photoinitiators with high two-photon absorption cross-sections, either commercially available ones (e.g. Irgacure 2959, Irgacure 369 and Michler's ketone) or custom-synthesized ones.[27–31] Hybrid organic–inorganic materials such as those based on organometallic polymers are highly promising due to their versatility of applications and properties. To date, organometallic materials incorporating Ge,[32] Ti,[33] V[34] and Zr[35] have been produced by LTPP. Hybrid materials incorporating Zr have been most widely used in the production of various 3D structures, from elements of microoptics,[36] photonics,[37] metamaterials,[2] to scaffolds for tissue engineering.[38,39] Tissue scaffolds fabricated out of this material have been shown to improve the proliferative potential, clonogenic capacity and differentiation potential of human mesenchymal stem cells.[40] The post-fabrication shrinkage of this material can be tuned by changing the duration of laser irradiation.[41] The polymer poly(2-(dimethylamino)ethyl methacrylate) can be used to further tune the mechanical properties of this material.[42] The *in vivo* biocompatibility of one of the iterations of the Zr-based hybrid material[35] was shown to be comparable to that of Polysorb™ 4-0 glycolide/lactide copolymer surgical sutures.[43] LTPP-produced Ti-based hybrid organic–inorganic materials have been less frequently described in the literature but have been used in the production of tissue scaffolds[44] and photonic crystals.[33] Ge-based hybrids have been used to fabricate photonic structures and microoptical elements such as photonic crystals, prisms and spatial polarization plates on either flat substrates or fibre tips.[32] V-based hybrids generated from pentavalent vanadium in vanadium triisopropoxide oxide (VOTIP) do not necessarily require photoinitiators to be added, since they absorb light and generate radicals which induce polymerization. Over the course of the polymerization V is reduced to its tetravalent form, while photonic crystal structures have been fabricated from this material as described earlier.[34]

Aluminium is another metal with great potential for biomedical applications. Its benefits include low cost, lightness and good biocompatibility. Poinern *et al.* have demonstrated the *in vitro* biocompatibility of anodic aluminium oxide membranes in culture with RK-13 rabbit kidney epithelial cells.[45] Furthermore, work by Kolekar *et al.* showed that Al doped hydroxyapatite was biocompatible with L929 mouse fibroblast cells *in vitro*.[46]

The development of complex tissue engineering products may require the integration of materials with different properties, yielding site-specific cellular adhesion, proliferation and differentiation, which motivates the creation of new polymers for precise microfabrication via LTPP. To the best of our knowledge, no LTPP-produced hybrid materials incorporating Al have yet been reported. Here, we report the use of LTPP to fabricate 3D structures based on a novel organometallic polymer containing Al. We then compare its spectroscopic and surface properties to those of Ti-, V- and Zr-incorporating organometallic polymers (the monomers used are displayed in Fig. 1) and relate them to their *in vitro* biocompatibilities.

EXPERIMENTAL

Materials

HCl (37% ultrapure) was purchased from AppliChem GmbH., Darmstadt, Germany. Aluminium isopropoxide (AIP) (≥98%) and toluene (ACS, ISO, Reag. Ph Eur) were purchased from Merck, Watford, UK. 3-(trimethoxysilyl)propyl methacrylate (MAPTMS) (98%), 4,4′-bis(diethylamino) benzophenone (DEABP) (≥99%), methacrylic acid (MAA) (99%), titanium(IV) isopropoxide (97%), VOTIP (Cat. #404926) and zirconium(IV) propoxide (70% in isopropanol) were purchased from Sigma-Aldrich, Gillingham, UK. Circular borosilicate cover glass slides 13 mm in diameter were purchased from Thermo Scientific, Warrington, UK. NIH/3T3 mouse embryo fibroblasts were purchased from ATCC, Kielpin, Poland. Dulbecco's phosphate buffered saline (DPBS), (ethylenediaminetetraacetic acid)–trypsin, foetal bovine serum, Iscove's modified Dulbecco's medium (IMDM) and penicillin–streptomycin mixture were purchased from Gibco, Thermo Scientific, Vilnius, Lithuania. 3-(4,5-dimethyl-2-thiazolyl)-2,5-diphenyl-2H-tetrazolium bromide (MTT) (98.9%) was purchased from Merck, Vilnius, Lithuania. Acridine orange (AO), ethidium bromide (EB) and dimethyl sulfoxide (DMSO) (≥99.5%) were purchased from Sigma-Aldrich, Gillingham, UK.

Synthesis

The Al-containing hybrid was synthesized by hydrolysis of MAPTMS using 0.1 mol L^{-1} HCl (10:1 v/v ratio) to 3-(trihydroxysilyl)propyl methacrylate (MAPTHS), stirring for 15 min. In parallel, AIP was dissolved in toluene in an ultrasonic bath for 15 min. MAA was then added to the AIP solution at a 1:1 AIP:MAA molar ratio. The two solutions of MAPTHS and MAA-AIP/toluene were mixed together at 1:1:4 AIP:MAA:MAPTHS molar ratio and stirred for *ca* 15 min. DEABP was used as a photoinitiator (1% by weight to the sum of AIP, MAA and MAPTHS) and stirred for 15 min.

Other hybrid materials were prepared in accordance with the literature. Zr-based hybrid materials were prepared with a molar

Polymer International published by John Wiley & Sons Ltd on behalf of Society of Chemical Industry.

ratio of 1:1:4 between zirconium propoxide, MAA and MAPTHS with 1% DEABP.[35] Ti-based hybrid materials were prepared with a 1:1:4 molar ratio between Ti isopropoxide:MAA:MAPTHS with 1% DEABP.[33] V-based hybrid materials were prepared with a 1:1 molar ratio between VOTIP and MAPTHS.[34]

Sample preparation

Cover glass slides were washed and silanized using MAPTMS according to a protocol adapted from Käpylä *et al.*[47] to ensure polymer bonding to the slides. Finally, the slides were washed again in ethanol to remove any uncrosslinked MAPTMS. Films were prepared by drop-casting a small volume of a precursor material on a slide and leaving the sample overnight in a fume hood in order for the solvent to evaporate. Samples were shielded from ambient light at all steps prior to photopolymerization to avoid unintentional crosslinking.

For energy dispersive X-ray (EDX) spectroscopy measurements, the slides were prepared in an analogous manner to those for structure fabrication. However, after solvent evaporation in a fume hood, the samples were polymerized using a UV lamp (UV-C, 40 W, Phillips, Amazon, Manchester, UK) for at least 2 h and then washed in a solvent for 15 min: Al hybrids were washed in toluene, Ti hybrids and Zr hybrids were washed in 4-methyl-2-pentanone and V hybrids were washed in isopropanol. Subsequently, all materials and reference glass slides were rinsed with ethanol and air-dried.

For biocompatibility testing, thin polymer films were prepared by spin-coating at 1500 rpm for 30 s on 13 mm circular glass slides and subsequently leaving them in a fume hood overnight for evaporation of the solvents. The films were polymerized using a 248 nm KrF excimer laser (30 ns pulse duration operating at 21 kV, 5 Hz repetition rate) for 2 min per sample or a UV lamp (UV-C, 40 W, Phillips, Amazon, Manchester, UK) for at least 2 h.

Prior to cell culture, the samples were washed in DPBS (three times for at least an hour each). The samples were disinfected under UV light in a laminar flow hood for at least 1 h per side to allow *in vitro* cell culture and were placed in sterile 24-well tissue culture plates.

Laser two-photon polymerization (multiphoton fabrication)

Two LTPP systems were used in structure fabrication. One is a commercially available Nanoscribe Photonic Professional GT (Nanoscribe GmbH/Eggenstein-Leopoldshafen, Baden-Wurttemberg/Germany) and based in the Department of Chemistry at Lancaster University. The system is based on a Topica FemtoFiber pro 100 fs pulsed 780 nm wavelength laser with a maximum power of 50 mW. A 63× 1.4 NA oil immersion Zeiss objective lens was used for fabrication. Structures were imported or programmed in DeScribe scripting software for controlling the fabrication process.

The other system was custom-built (described previously)[48] and based at FORTH-IESL. A schematic representation is given in Fig. 2. A Ti:sapphire laser (Femtolasers Fusion) was used as a light source, operating at 780 nm central wavelength with 20 fs pulse duration and 75 MHz repetition rate. The average laser power was set between 10 and 100 mW using an attenuator (Altechna). The sample was positioned on piezoelectric stages and the laser beam was guided using a galvanometric mirror scanner (Scanlabs Hurryscan II) through a 40× 0.95 NA (Zeiss, Plan-Apochromat) or an oil immersion 100× 1.4 NA (Zeiss, Plan-Apochromat) objective lens. The process of fabrication was controlled by SAMLight (SCAPS) software. Writing speeds between 0.1 and 1 mm s^{-1} were found to be suitable for this purpose.

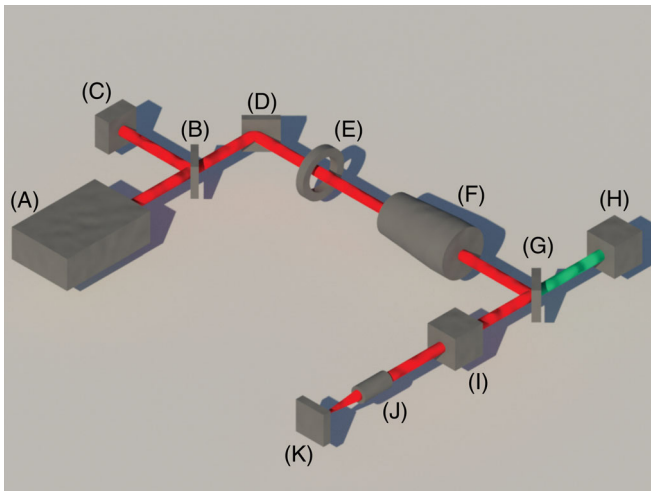

Figure 2. A schematic representation of the LTPP system used at FORTH-IESL: (A) the laser; (B) a beam splitter; (C) spectrum analyser; (D) mirror; (E) an attenuator; (F) a telescope; (G) a dichroic mirror; (H) a CCD camera for real-time observation of the fabrication process; (I) a galvo-scanner; (J) an objective lens; (K) the sample stage with light-emitting diode illumination for the CCD camera.

Scanning electron microscopy (SEM)

Samples were washed in toluene for 15 min and then rinsed with isopropanol and air-dried. Prior to imaging the samples were sputter coated with a 10 nm layer of gold. The structures were observed using either a JEOL JSM−6390L V operating at 15 kV or a JEOL JSM 7800F scanning electron microscope (JEOL, Welwyn Garden City, UK) operating at 10–15 kV.

EDX analysis

For qualitative EDX analysis, the samples were sputter coated with a layer of gold (60 s, 20 mA, 8×10^{-2} mBar, *ca* 5 nm) using a Quorum Q150RES sputter coater (Quorum Technologies Ltd) and then investigated using a field-emission SEM JEOL JSM 7800F with an EDX system (X-Max50, Oxford Instruments, Abingdon, UK) at 10 mm working distance and 10 kV voltage mounted on a brass JEOL holder with 25 mm carbon tables (G3348N, Agar Scientific, Stansted, UK). Three measurements were performed per sample and average results are presented.

X-ray photoelectron spectroscopy (XPS) analysis

The XPS analyses were carried out with a Kratos Axis Supra spectrometer (Kratos Analytical, Manchester, UK) using a monochromatic Al Kα source (20 mA, 15 kV). XPS can detect all elements except hydrogen and helium, probes the surface of the sample to a depth of 5–7 nm and has detection limits ranging from 0.001 to 0.5 at% depending on the element. The instrument work function was calibrated to give a binding energy of 83.96 eV for the Au 4f7/2 line for metallic gold and the spectrometer dispersion was adjusted to give a binding energy of 932.62 eV for the Cu 2p3/2 line of metallic copper. The Kratos charge neutralizer system was used on all specimens. Survey scan analyses were carried out with an analysis area of 300 × 700 µm and a pass energy of 160 eV. High resolution analyses were carried out with an analysis area of 300 × 700 µm and a pass energy of 20 eV. Spectra have been charge corrected to the main line of the carbon 1s spectrum (adventitious carbon) set to 285.0 eV.

Contact angle measurements

Two microlitre droplets were placed on spin-coated sample slides or ethanol-washed reference glass slides and pictures were taken using a Krüss EasyDrop contact angle measurement system (KRÜSS GmbH Wissenschaftliche Laborgeräte, Hamburg, Germany) and analysed using proprietary software. The sample chamber temperature was kept constant at 21 °C using a LabTech H50-500 water chiller (Thermo Scientific, Vilnius, Lithuania). A total of five measurements per material were performed. Results are presented as mean ± standard deviation.

Polymer extracts

Polymer samples were spin-coated and polymerized under UV as in the case with biocompatibility testing. The samples were then incubated in DPBS on a plate shaker at 40 rpm for 24 h at room temperature. The PBS containing spin-coated polymer extracts was subsequently aspirated to new tissue culture plate wells and heated for 5 h at 80 °C until the water had evaporated.

Polymer extract metal content analysis via inductively coupled plasma optical emission spectrometry (ICP-OES)

Measurements were performed using an Agilent 5100 VDV inductively coupled plasma optical emission spectrometer (Agilent Technologies UK Limited, Cheadle, UK) in axial mode. The sample introduction system consisted of a glass concentric nebuliser, a glass cyclonic double pass spray chamber and a demountable dual view quartz 1.8 mm torch. The solid samples were dissolved directly from the well-plate locations in dilute nitric acid (2% w/v) with several washings and made up to the final volume (10 mL) with dilute nitric acid (2% w/v). Calibration curves of the target elements Al, Ti, V, Zr, Na and P were prepared between 1 and 100 ppm using single element standards (Sigma-Aldrich, TraceCERT, 2% HNO_3), with the exception of P (Alfa Aesar, SpecPure, 5% HNO_3). All blanks were prepared from the original stock of dilute nitric acid (2% w/v) used to prepare standards and samples. All blanks, standards and samples were prepared with yttrium internal standard (1 ppm, Sigma-Aldrich, TraceCERT, 2% HNO_3).

Cell culture and maintenance

All biocompatibility tests were performed on NIH/3T3 mouse embryo fibroblasts from American Type Culture Collection (ATCC, Manassas, USA). The cells were cultured in IMDM supplemented with 10% foetal bovine albumin, 100 U mL^{-1} penicillin and 100 µg mL^{-1} streptomycin. The cells were maintained at 37 °C with 5% CO_2 and passaged every 3–4 days. The passage procedure started with washing the monolayer of cells once with DPBS followed by 0.25% (ethylenediaminetetraacetic acid)–trypsin treatment for 1 min. Detached cells would later be collected in full medium and passaged in a new flask.

Polymer extract toxicity

Polymer samples were spin-coated and polymerized under UV as described for the biocompatibility testing. The samples were then incubated in a full cell growth medium (containing serum and antibiotics) for 24 h at room temperature. The medium containing spin-coated polymer extracts was subsequently aspirated and used on NIH/3T3 fibroblasts grown in a monolayer for 24 h. They were cultured for another 24 h with normal medium as a reference point at 37 °C with 5% CO_2 atmosphere. An MTT assay was then performed on the cells grown in extract-containing media.

MTT assay and light microscopy

NIH/3T3 mouse embryo fibroblasts were seeded on spin-coated samples at a density of 20 000 cells mL^{-1} per sample, using glass slides as control. The samples were incubated at 37 °C with 5% CO_2 atmosphere. Light microscopy images were taken after 96 h of culture on each surface and cellular morphology was qualitatively assessed. After 120 h of culture, the samples were transferred to new tissue culture plates, where they were treated with 0.2 mg mL^{-1} and incubated for 1 h at 37 °C. The MTT solution was then carefully replaced with 200 µL of DMSO to solubilize the formazan. The optical density at 545 nm was measured by using an automatic microplate reader. Results were calculated as the ratio between cells grown on hybrid materials and glass. A total of 40 samples per material were prepared and split into eight independent experiments with $n = 5$ per experiment. Results are presented as averages ± standard error.

Analysis of cell death

NIH/3T3 mouse embryo fibroblasts were seeded and cultured as described in the previous section. The type of cell death was determined microscopically by using two fluorescent dyes, AO/EB, as described by Mercille and Massie.[49] Briefly, cells from the different samples and glass slides were individually collected, centrifuged and suspended in 20 µL of fresh IMDM supplemented with foetal bovine serum and antibiotics and stained with 4 µL of AO (100 µg mL^{-1})/EB (100 µg mL^{-1}) solution for 5 min. Then, the cells were observed using an Olympus IX51 inverted fluorescence microscope with an X-Cite 120PC Q UV lamp (Lumen Dynamics) and photographed using an ExiBlue camera (QImaging) with proprietary imaging software. 100 cells were counted per sample and split into three categories based on their nuclear and membrane integrity: live (cells with uniform green nucleus), apoptotic (cells with fragmented nuclei that fluoresce green (early apoptosis) or orange (late apoptosis)) and necrotic (intact, bright orange stained nuclei). Five independent experiments were carried out and averages ± standard deviations are presented.

Statistical analysis

Statistical analysis was performed using RStudio® (version 1.1.383 for Mac running on R 3.4.2) and plotted using the ggplot2 package. The data are presented as either mean ± standard error or standard deviation. Statistical significance was assessed using one-way ANOVA and Tukey's honestly significant difference (HSD) *post hoc* test. Differences between groups were considered to be significant for $P < 0.05$ (*), $P < 0.01$ (**) and $P < 0.001$ (***).

RESULTS AND DISCUSSION

Material preparation

The Ti, V and Zr formulations were adapted from the literature.[33–35] The preparation procedure of the Al hybrid is analogous to those of other hybrid materials that have been used for LTPP except that the metal propoxide comes in a powder form, so it has to be dissolved first. Several solvents were tested for this purpose, including ethanol, isopropanol, hexane, cyclohexane and benzene, but the best solubility was obtained using toluene. The resulting material is a clear liquid with a yellow hue because of the presence of DEABP. After evaporation of the solvent, the material transitions to a viscous gel-like state. Gelation reduces structural distortions that would arise during fabrication in a liquid due to vibrations, diffusion and stage movement in some LTPP systems.

Polym Int 2019; **68**: 1928–1940
Polymer International published by John Wiley & Sons Ltd on behalf of Society of Chemical Industry.

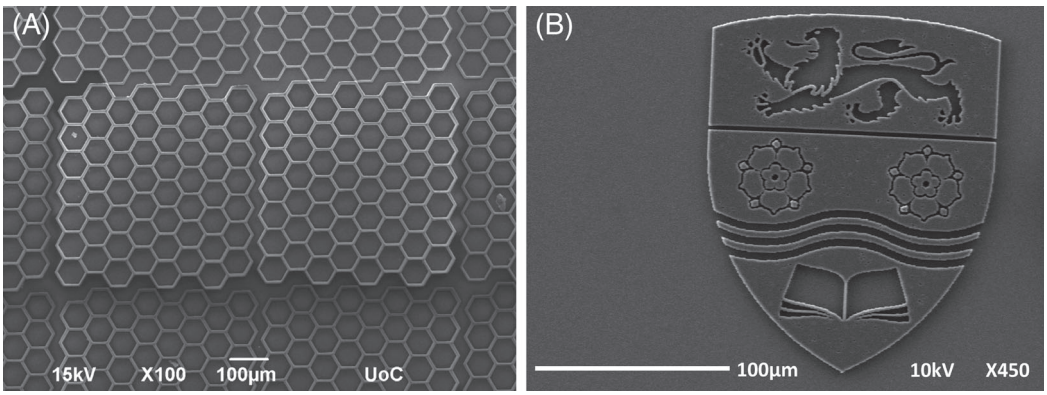

Figure 3. 2D structures fabricated out of the Al hybrid material: (A) honeycomb patterns fabricated using the custom-built LTPP system with a 40× 0.95 NA objective lens; (B) the coat of arms of Lancaster University fabricated using the Nanoscribe® system with a 63× 1.4 NA oil immersion lens.

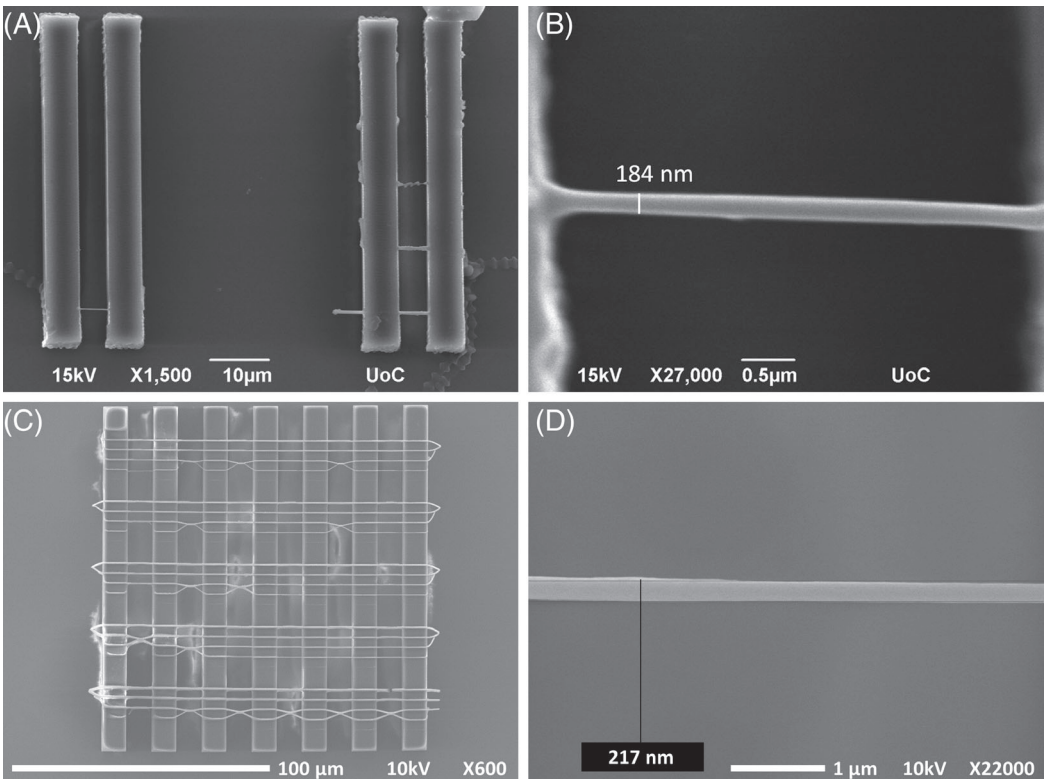

Figure 4. Support structures with suspended lines between them fabricated out of the Al hybrid material: (A), (B) structures fabricated using the custom-built LTPP system with a 100× 1.4 NA oil immersion lens at different magnifications; (C), (D) structures fabricated using the Nanoscribe® system with the 63× 1.4 NA oil immersion lens. Lines with resolutions down to around 200 nm were reproducibly fabricated using both systems.

Material iterations with different proportions between the components were tested with the AIP:MAA molar ratio remaining constant at 1:1 and AIP:MAPTHS being 1:1, 1:4 or 1:9. All the combinations were shown to be polymerizable in 3D, but 1:4 AIP:MAPTHS was chosen to be the same as in Ti and Zr hybrid materials.

Laser two-photon polymerization (multiphoton fabrication)

LTPP of hybrid organometallic polymers based on Ti,[33] V[34] and Zr[35] have been described in the literature. Both Ti and Zr hybrid materials have been used to produce scaffolds for tissue engineering.[24,44] Consequently, in this work we focused on investigating the properties and structurability of the novel Al hybrid material. The Al hybrid material is transparent, while the intrinsic photoinitiator renders it fluorescent upon irradiation with a laser. This makes finding the interface between the material and the glass slide as straightforward as with commercially available photoresists such as OrmoComp® or OrmoClear®. We first tested the Al hybrid organometallic polymer on both the Nanoscribe® and the custom-built LTPP systems in an attempt to fabricate 2D structures (Fig. 3). The printing of each of these structures took no more than 10 min.

Having shown that it is possible to fabricate high quality structures with minimal spatial distortions (Fig. 3), we modelled and fabricated suspended lines with varying laser power and scanning speed between bulky support structures to assess maximum resolution of the Al hybrid (Fig. 4). Lines that survived the development process reproducibly reached <200 nm in width

Polymer International published by John Wiley & Sons Ltd on behalf of Society of Chemical Industry.

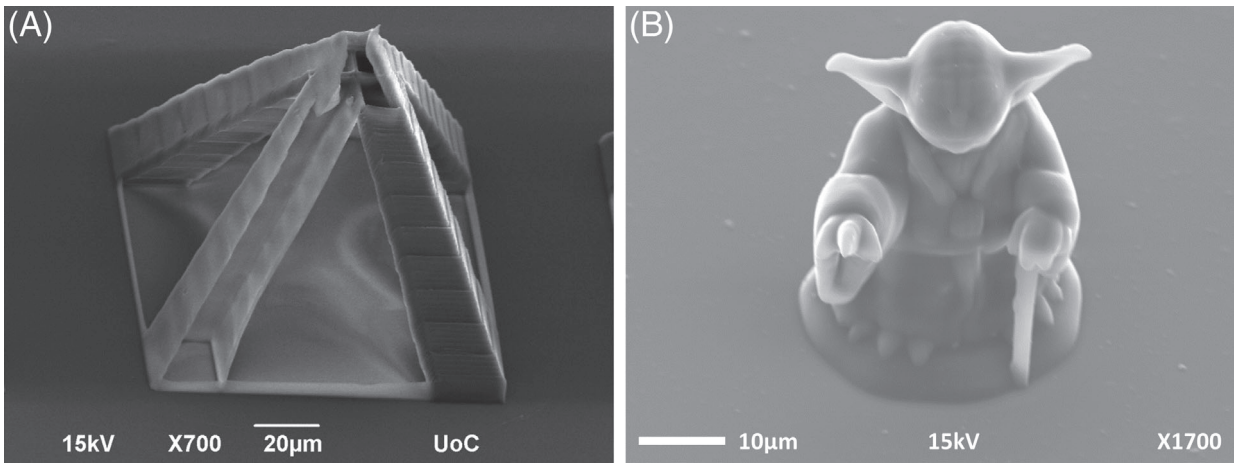

Figure 5. 3D structures fabricated out of the Al hybrid material: (A) a hollow pyramid shell fabricated using the custom-built LTPP system with a 100× 1.4 NA oil immersion lens; (B) a micro-Yoda fabricated using the Nanoscribe® system with a 63× 1.4 NA oil immersion lens.

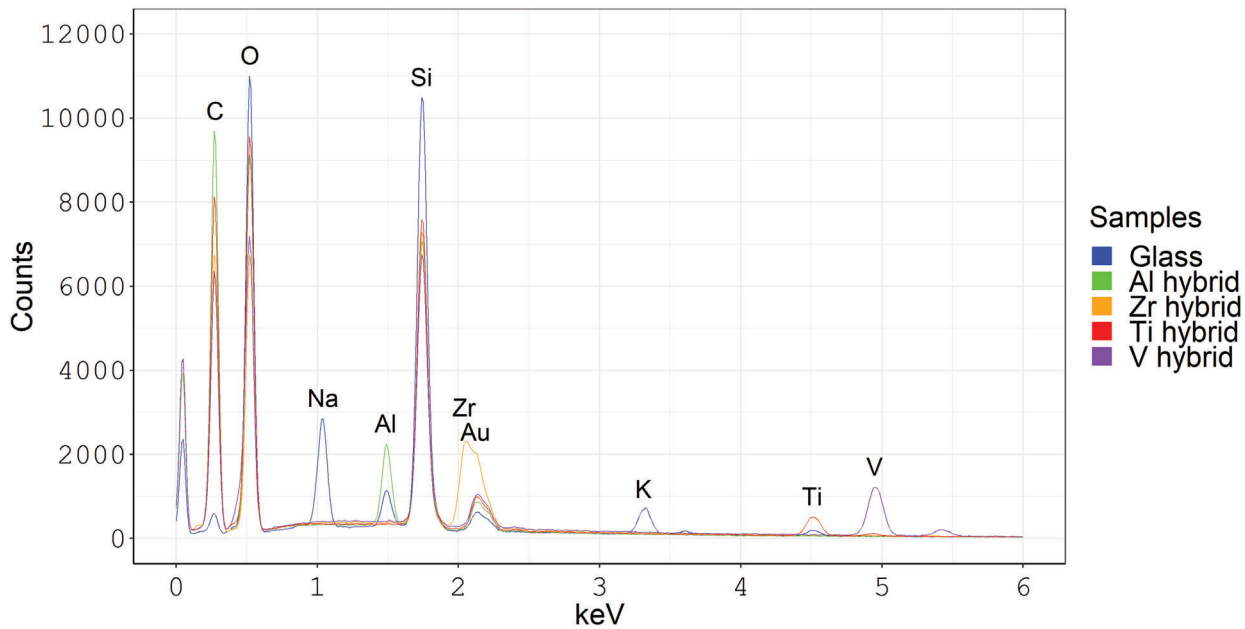

Figure 6. EDX spectra of the different organometallic hybrid polymers containing Al, Ti, V and Zr, and the borosilicate glass control.

using the 100× 1.4 NA oil immersion lens on the custom-built LTPP system and <250 nm using a 63× 1.4 NA oil immersion lens on the Nanoscribe® system. The result is comparable to resolutions reached using other hybrid organic–inorganic materials via LTPP. 3D structures were fabricated on both systems (Figs 4 and 5), taking no more than 30 min each. The structures survived the development and washing processes with minimal shrinkage or deformation. The hollow pyramid and Yoda structures (Fig. 5) demonstrate the relative rigidity of the material.

EDX analysis

EDX spectroscopy was performed on all the tested materials based on Al, Ti, V and Zr in order to compare their chemical constituents. The analysis was performed on drop-cast films and confirmed the presence of metals in the organometallic materials (Fig. 6). The films were relatively thick (of the order of hundreds of microns), so the X-ray signals were most likely being generated by the materials. The same type of glass slides on which the materials were drop-cast were used as references. The Al hybrid showed a peak at around 1.5 keV that had 1.96 times greater X-ray photon count than that measured in glass, indicating the presence of Al (characteristic Kα = 1.486 keV). In the case of the V hybrid, a peak at around 5 keV indicates the presence of V (characteristic Kα = 4.949 keV and Lα = 0.511 keV) with X-ray photon count differing around 20 times from that of glass at 4.949 keV. The Lα of V was not visible due to overlap with the Kα of O. Significantly larger amounts of Ti were found in Ti hybrid material compared to control glass slides, with X-ray photon count at Kα = 4.508 keV being around 2.7 times greater than in reference glass. Finally, a peak at 2 keV indicates the presence of Zr (characteristic Lα = 2.042 keV) in the Zr hybrid with X-ray photon counts differing from glass by 10.7 times. The presence of gold due to the coating method was confirmed in all samples at 2.120 keV. Signals from K and Na were only detectable in the glass, confirming that the resin thickness was high enough for the X-rays to be generated within the resins.

Polymer International published by John Wiley & Sons Ltd on behalf of Society of Chemical Industry.

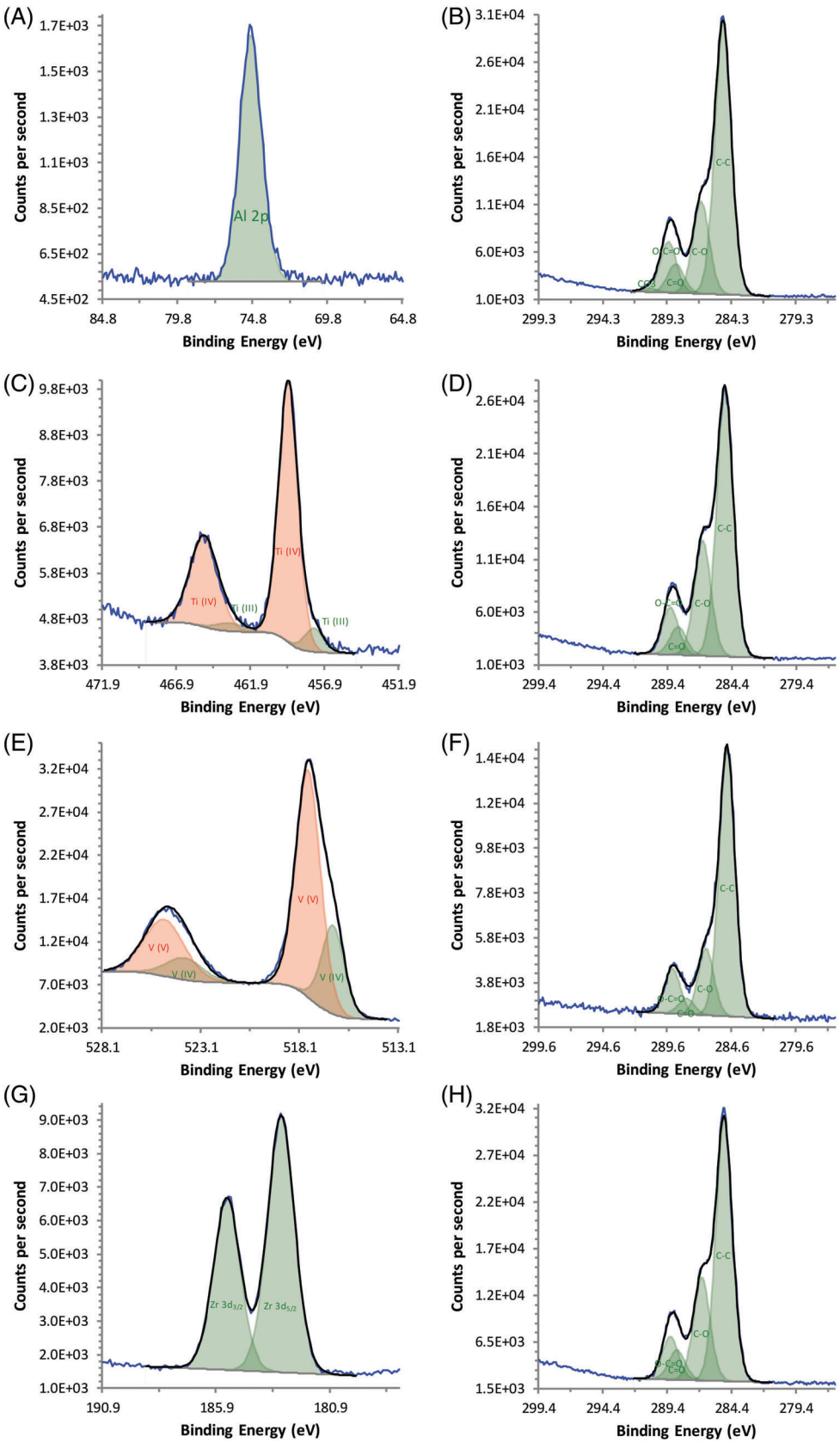

Figure 7. XPS spectra of the different organometallic hybrid polymers containing Al (A), (B), Ti (C), (D), V (E), (F) and Zr (G), (H). (A), (C), (E) and (G) show the oxidation state of the metals in the polymers and relative proportions thereof. (B), (D), (F), (H) show the compositions of carbonaceous species in the polymers and relative proportions thereof.

Polymer International published by John Wiley & Sons Ltd on behalf of Society of Chemical Industry.

Table 1. A summary of the surface compositions (%) of the metal-based species from the representative large area survey XPS spectrum of the various samples

	Substrate			
Metal	Al	Ti	V	Zr
Binding energy (eV)	74.90	457.65 and 459.37	516.31 and 517.63	183.07
Possible species	$Al(OH)_3$ or AlO(OH)	Ti(III) or Ti(IV)	V(IV) or V(V)	Zr(IV)

Table 2. A summary of the surface compositions (%) of the C-based species from the representative large area survey XPS spectrum of the various samples

	Substrate			
C 1s	Al	Ti	V	Zr
C–C	60.63	58.31	67.75	59.78
C–O	20.67	25.22	16.89	23.57
C=O	6.46	6.18	4.02	6.82
O–C=O	11.37	10.30	11.33	9.83
$(C–O)_3$	0.87	0.00	0.00	0.00

XPS analysis

Akin to EDX analysis, XPS analysis (Fig. 7, Tables 1 and 2, Figs S1–S12 and Tables S1–S3) confirms the presence of the metals in the polymer films. XPS also offers insight into the oxidation state of the metals (and relative proportions thereof, Fig. 7 and Table 1) and carbonaceous species (and relative proportions thereof, Fig. 7 and Table 2). Interestingly, XPS shows that the polymers for Al-, Ti- and Zr-containing polymers have similar compositions of carbonaceous species. By comparison, the V-containing polymer compositions had lower C=O content which is related to their content of MAA which would bind the metal cation through interaction with the anionic carboxylates from MAA moieties (i.e. weaker metal ion binding than the other polymers).

Contact angle measurements

The results show that the hybrid organic–inorganic materials had higher contact angles than those of glass slides (Fig. 8). We found that the average contact angle of glass slides prior to washing was 64° and 39° after ethanol washing and air-drying. The Al and Zr hybrid materials had contact angles of *ca* 72° and 71°, respectively. The Ti hybrid material was more hydrophobic, with a contact angle of around 90°. The V hybrid material had the highest contact angle of *ca* 102°.

Biocompatibility assessment

NIH/3T3 fibroblasts were seeded on the surfaces to investigate their biocompatibility. Light microscopy images were taken after 96 h of culture. Healthy fibroblasts tend to be spindle-shaped, while non-viable cells tend to become rounded and detach from the surface. We observed that after 96 h spindle-shaped cells can be found on all surfaces except for the V hybrids (Fig. 9).

All surfaces supported cell adhesion and proliferation (probably via protein-adsorption-mediated adhesion in line with other biomaterials) with the exception of the V-containing hybrid which is likely to be because vanadium oxides are more toxic than vanadium in its elemental form. To quantify the biocompatibility results, MTT assays were performed after 120 h of culture. The data obtained are presented as a ratio of optical density of cells grown on the hybrid materials to that of cells grown on glass (Fig. 10). The total cellular metabolic activity is proportional to the optical density. NIH/3T3 mouse fibroblasts tended to attach and proliferate on all surfaces except the V hybrid material. We observed that the cells tended to have the highest metabolic activity on the Zr-based hybrid material. These findings support the biocompatibility notion of this material together with *in vivo* studies that have previously shown the material to be of comparable biocompatibility to that of a surgical suture composed of glycolide/lactide (Polysorb™ 4–0).[43] There were no significant differences between the rates of total cellular metabolism on the

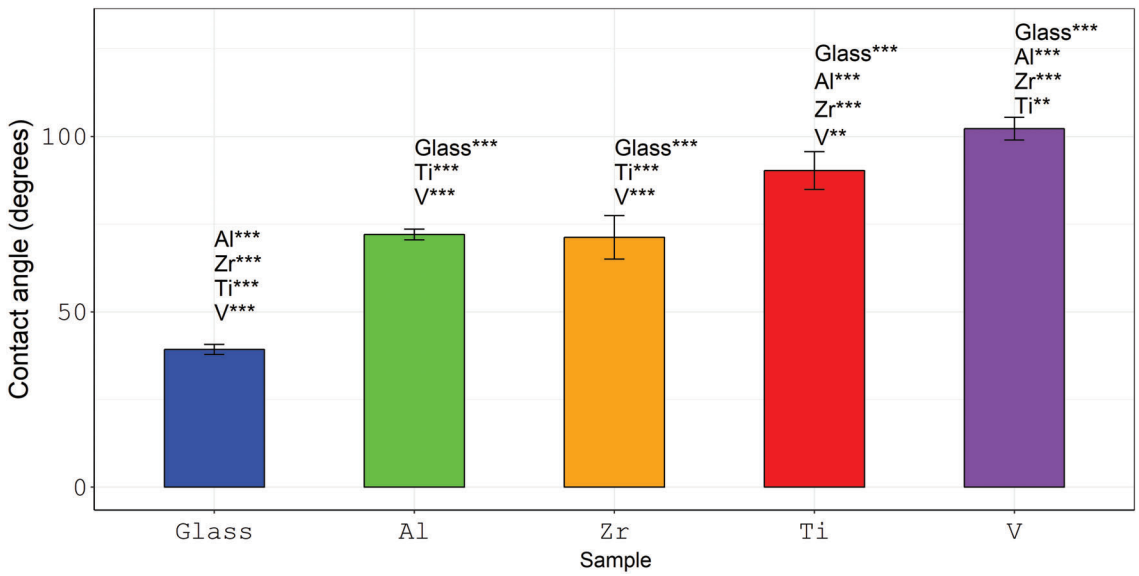

Figure 8. Water contact angles ± standard deviation. Al, Ti, V and Zr correspond to Al, Ti, V and Zr hybrid materials; glass was used as a control. $^{**}P < 0.01$, $^{***}P < 0.001$, glass was significantly different from all other surfaces with $P < 0.001$.

Polymer International published by John Wiley & Sons Ltd on behalf of Society of Chemical Industry.

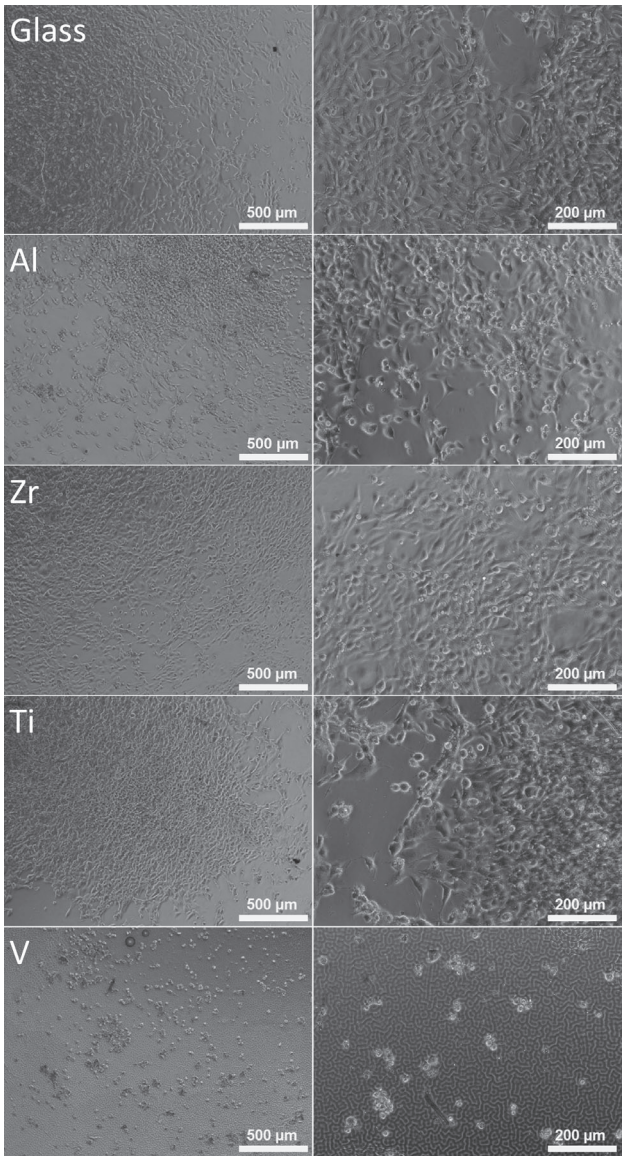

Figure 9. NIH/3T3 fibroblasts grown on the organometallic polymer materials and control glass surfaces. Pictures were taken 96 h after cell seeding using both 4× and 10× objective lenses on an inverted light microscope. Cellular morphology is healthy in glass and Al-, Zr- and Ti-containing polymers. However, none of the cells was attached to the V-containing polymers after 96 h (probably due to leaching of V from the films).

Al and Ti hybrids. The Zr hybrid was significantly more supportive of cell growth than Al- and Ti-based hybrids. The preliminary studies de-risk a more extensive (and costly) investigation into the cell–surface interactions and surface protein adsorption that would underpin the use of the materials in tissue engineering or other biological applications.

To investigate whether the toxicity of the V-containing polymers is due to their surface properties or to some components being washed out into the medium, we used sample extracts to treat cells grown in a monolayer. The results are presented in Fig. 11 showing that the Al extract was significantly ($P < 0.05$) beneficial to the cell culture, while control, Ti and Zr sample extracts did not have significantly different effects on cellular viability. The V sample extract was highly toxic to the cell monolayer with $P < 0.001$ compared to all other sample extracts. This suggests non-crosslinked metal ions are washed out into the medium, thus contributing to the toxicity towards cells grown *in vitro* (which correlates with the ICP-OES data).

To assess the mechanism of cell death, differential staining with AO/EB was applied and the numbers of live, apoptotic and necrotic cells were calculated. Results confirm that the most cytotoxic surface for cell culture was the V hybrid (Fig. 12). The majority of cells had undergone necrosis after 24 h of culture, while after 96 h and 120 h there were virtually no living cells remaining on these surfaces. Necrosis was a much more prevalent type of cell death on all of the surfaces compared to apoptosis. We investigated whether there were any significant differences between the numbers of live cells on the surfaces. We observed that the number of live cells on all samples (except for the V hybrids) was between 60% and 80% at all time points (24, 96 and 120 h).

The V hybrid materials displayed the highest cytotoxicity with the majority of cells dying via necrosis. Statistically significant ($P < 0.001$) differences were found between all samples compared to the V hybrid material in terms of the number of live and necrotic cells (Fig. 12), consistent with very low optical density in the MTT assay and ICP-OES confirmed leaching of the V (Fig. 13). This is in accordance with previously reported work showing the toxicity of V both in its elemental and oxide forms.[50] No statistically significant differences were observed between the numbers of apoptotic cells (Fig. 12). Other statistically significant differences between the numbers of live and necrotic cells on the surfaces are summarized in Table 3.

Al-, Ti- and Zr-based hybrid organometallic polymers showed good biocompatibility *in vitro*. The numbers of live, apoptotic and necrotic cells on all these surfaces were comparable at every time point (after 24, 96 and 120 h). However, the highest metabolic rate according to the MTT assay was found on the Zr hybrid.

Increased surface hydrophobicity improves irreversible protein adsorption with albumin being one of the first proteins to reach the surface[51] which does not have cell adhesion motifs, possibly having a negative impact on material biocompatibility.

Ti is attractive due to its mechanical strength and biological inertness as its alloys are widely used in dental[52] and orthopaedic[53] applications. Zr-based biomaterials are also widely used in the clinic, and zirconia ceramics are a class of biocompatible materials with comparable properties to those of Ti.[54] Since both Ti and Zr are being widely used for biomedical applications, hybrid organometallic polymers containing these metals are worthy of investigation.

Good *in vitro* biocompatibility has been demonstrated in many 3D printing materials ranging from hydroxyapatites[55] to organic polymers, such as polyvinyl alcohol reinforced with cellulose nanofibrils.[56] However, a limited number of the existing biocompatible materials offer the possibility of reproducible sub-micron structure fabrication in 3D.

Al is not used for implant fabrication due to its solubility under acidic conditions as well as limited mechanical strength. Al^{3+} has also been linked to Alzheimer's disease and other types of neurodegeneration.[57] However, in chemically stable and inert structures, the presence of Al is not considered to be dangerous, and it is noteworthy that Al is a part of many Ti alloys used in biomedical applications.[58] While the toxicity of Al^{3+} is known, compounds of Al such as oxides and hydroxides are widely used as food additives, pharmaceuticals and personal care products and are considered safe.[59] Our data presented in this work confirm that Al-containing polymers have potential to be used in biomedical applications.

Polymer International published by John Wiley & Sons Ltd on behalf of Society of Chemical Industry.

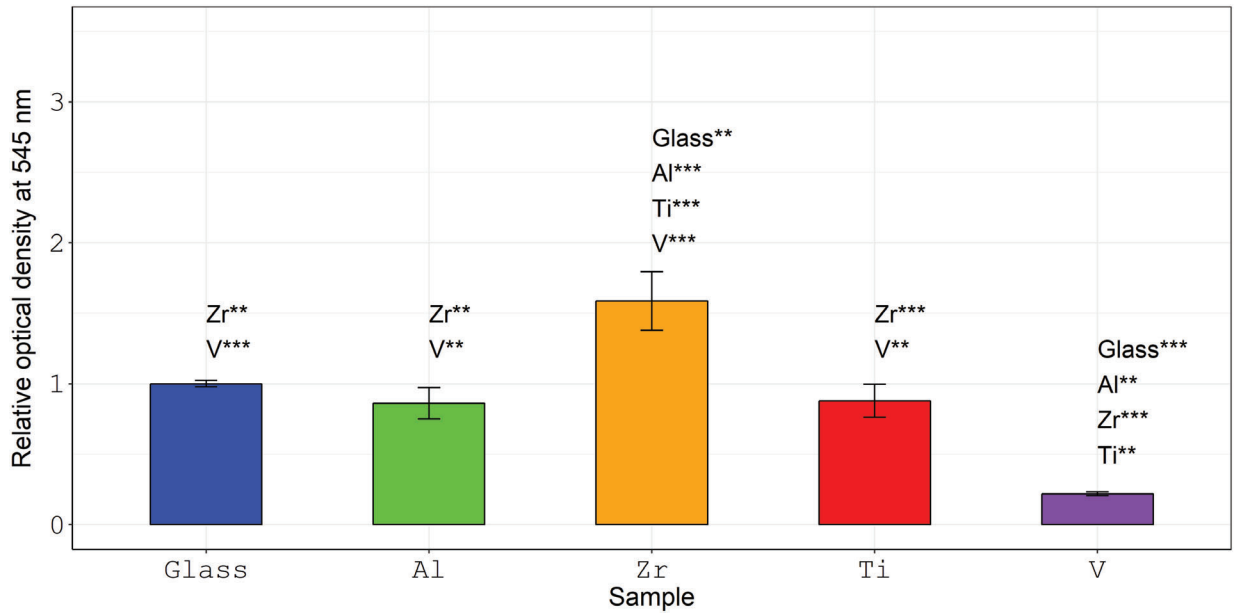

Figure 10. Relative optical density as measured via MTT after 120 h of cell culture. The optical density is directly proportional to the total metabolic activity of cells on each surface. Results are presented as absorption ratio to that of glass ± standard error. $^{**}P < 0.01$, $^{***}P < 0.001$.

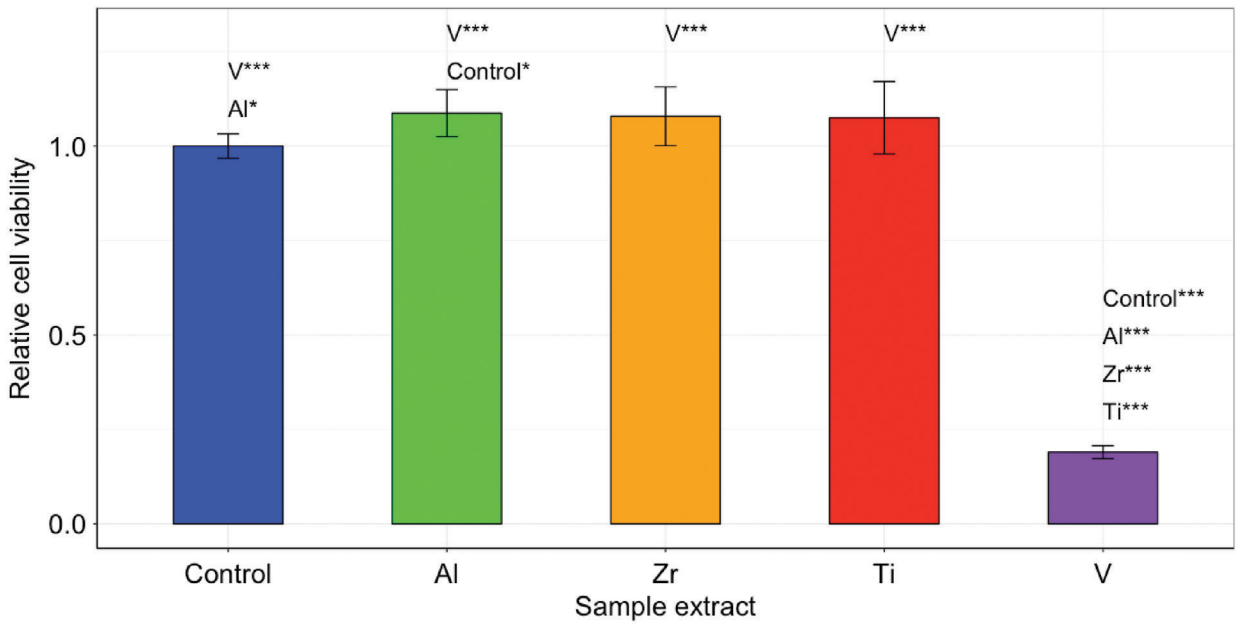

Figure 11. Cells cultured in media containing the polymer sample extracts. Results are presented as absorption ratio to that of glass ± standard deviation. Al and control surfaces had a significant difference with $^{*}P < 0.05$, while V was significantly different from all other surfaces with $^{***}P < 0.001$.

The use of hybrid organometallic polymer-based materials as implants is a relatively new concept and is being more thoroughly investigated due to the possibility of 3D microstructure fabrication. Good *in vitro* biocompatibility has been demonstrated in many 3D printing materials, ranging from hydroxyapatites[55] to organic polymers, such as polyvinyl alcohol reinforced with cellulose nanofibrils.[56] However, a limited number of the existing biocompatible materials offer the possibility of reproducible sub-micron structure fabrication in 3D. Moreover, integration of several different materials with varying properties will allow bioengineers to finely tune both the mechanical and biological properties of this next generation of implants.

CONCLUSIONS

A hybrid organic–inorganic material based on Al has been developed for laser 3D fabrication purposes. LTPP experiments show that the organometallic polymer-based materials can be used to easily fabricate 2D and 3D structures. Low shrinkage of the material allows high resolution (down to 200 nm) structures to be made, which is on a comparable scale to other hybrid organic–inorganic materials.

Biocompatibility testing shows that Al-, Ti- and Zr-containing organometallic polymers support NIH/3T3 fibroblast growth. Cell viability on these surfaces was comparable to that of control glass surfaces. We observed that the rate of metabolism on Al-

Polymer International published by John Wiley & Sons Ltd on behalf of Society of Chemical Industry.

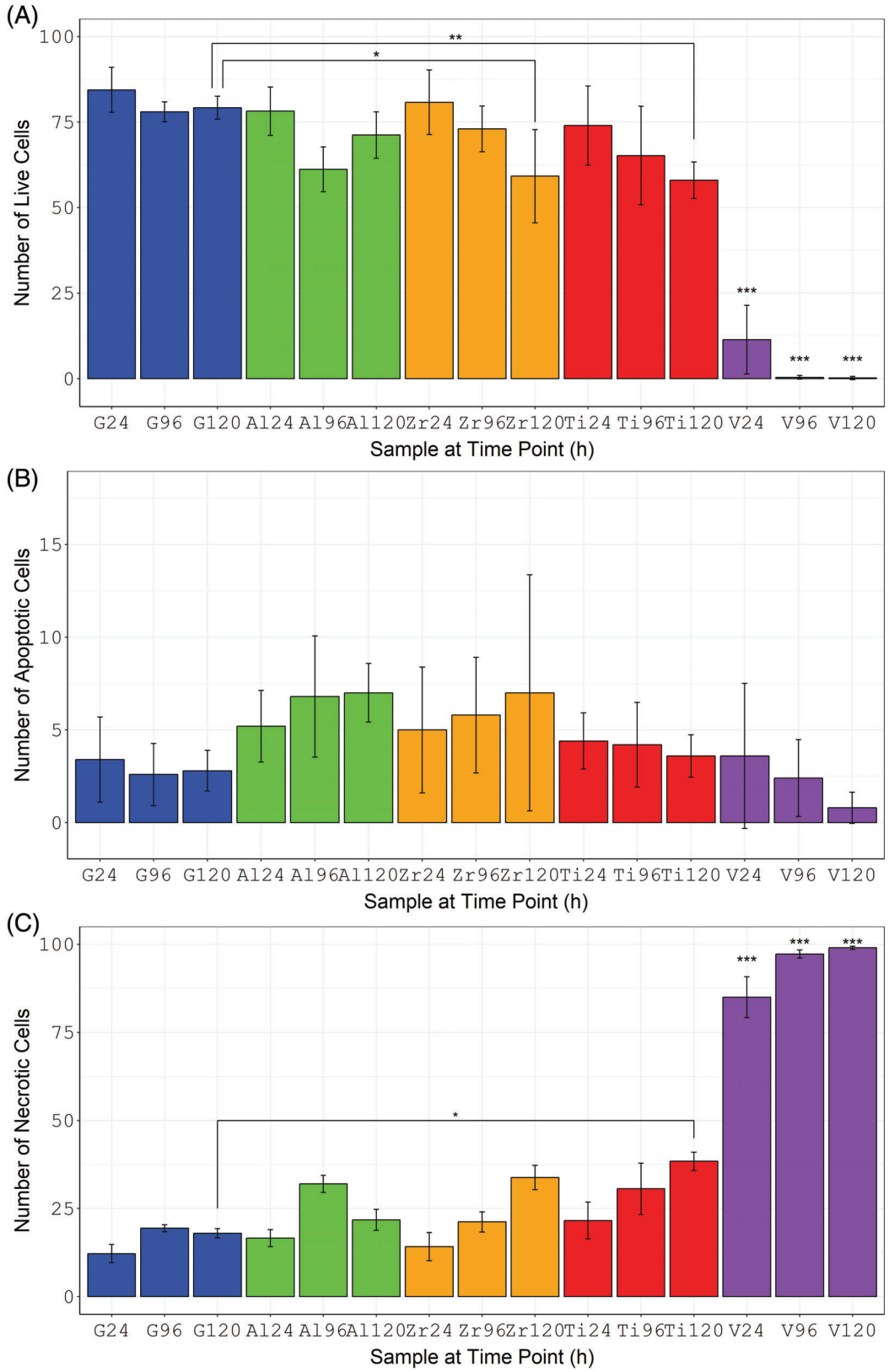

Figure 12. Number of live, apoptotic and necrotic cells on glass, Al, Zr, Ti and V organometallic hybrid materials after 24, 96 and 120 h of culture determined via acridine orange/ethidium bromide staining. Five samples per material per time point were used to calculate 100 cells on each. The results are presented as averages ± standard deviation. Statistical analysis was performed between all groups; however, only differences between corresponding time points are presented. In both live and necrotic cell cases, the results for V hybrids were significantly different from all other surfaces with a P value of <0.001 (***). *$P < 0.05$, **$P < 0.01$, ***$P < 0.001$.

Polymer International published by John Wiley & Sons Ltd on behalf of Society of Chemical Industry.

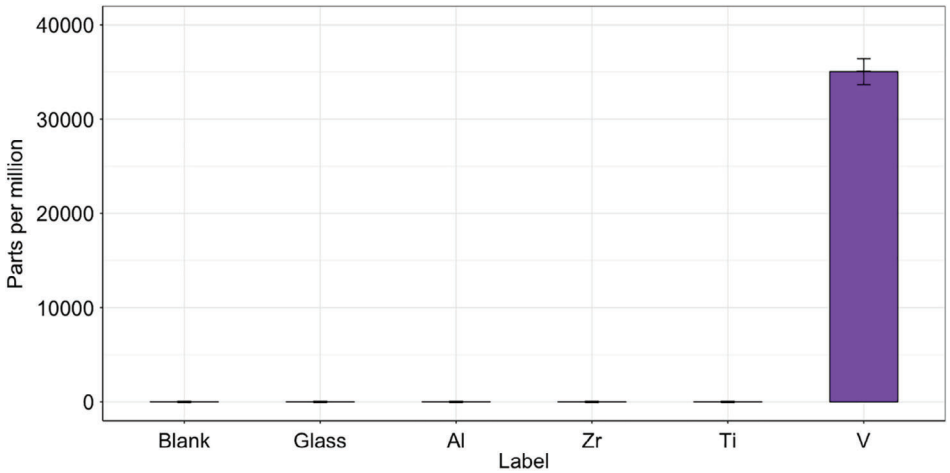

Figure 13. ICP-OES data of extracts from Al, Zr, Ti and V organometallic hybrid materials.

Table 3. A summary of statistically significant differences not presented in Fig. 10

Comparison	Live	Necrotic
Al96-G24	**	*
Zr120-G24	***	**
Ti96-G24	*	*
Ti120-G24	***	***
Zr120-G96	*	–
Ti120-G96	*	*
Zr120-Al24	*	**
Ti120-Al24	*	–
Zr24-Al96	*	*
Zr120-Zr24	**	*
Ti120-Zr24	**	***

*$P < 0.05$.
**$P < 0.01$.
***$P < 0.001$.

and Ti-containing materials was comparable to that of glass, while Zr supported a significantly higher proliferation rate of NIH/3T3 fibroblasts. Cellular morphology was normal on Al-, Zr- and Ti-containing materials. The V-containing organometallic polymer was shown to be toxic to cells and induced necrosis. The Al-, Zr- and Ti- containing organometallic polymers have been shown to be promising candidates for tissue engineering applications. However, an extensive investigation of cell topography responses, taking into account the expression of adhesion proteins, long-term viability and biodegradability studies of the materials are needed if they are to be used for tissue engineering or other *in vivo* applications, and the specific tissue niches in which they may be applicable based on the conditions to which the materials would be exposed *in vivo* (fluid flow, mechanical stress, tissue mechanics etc.).

ACKNOWLEDGEMENTS

We thank Dr Maria Farsari and Dr Anthi Ranella from the Institute of Electronic Structure and Laser, Foundation for Research and Technology – Hellas (FORTH-IESL) for providing E. B. with access to the laser two-photon polymerization and cell culture facilities, and Ms Aleka Manousaki from the University of Crete for SEM imaging. We thank Dr Gintaras Valinčius and Dr Tadas Ragaliauskas for access to spin-coating and contact angle measurement equipment, and Dr Virginija Bukelskienė for insightful discussions.

The work was supported by the European Commission via the Marie Skłodowska-Curie research fellowship programme AngioMatTrain (Grant agreement 317304) and a Lancaster University Faculty of Science and Technology Early Career Internal Grant, a Royal Society Research Grant (RG160449) and an EPSRC First Grant (EP/R003823/1).

SUPPORTING INFORMATION

Supporting information may be found in the online version of this article.

REFERENCES

1 Deubel M, von Freymann G, Wegener M, Pereira S, Busch K and Soukoulis CM, *Nat Mater* **3**:444–447 (2004). https://doi.org/10.1038/nmat1155.
2 Kenanakis G, Xomalis A, Selimis A, Vamvakaki M, Farsari M, Kafesaki M *et al.*, *ACS Photon* **2**:287–294 (2015). https://doi.org/10.1021/ph5003818.
3 Galajda P and Ormos P, *Appl Phys Lett* **78**:249–251 (2001). https://doi.org/10.1063/1.1339258.
4 Lee W, Pruzinsky SA and Braun PV, *Adv Mater* **14**:271–274 (2002). https://doi.org/10.1002/1521-4095.
5 Guo R, Xiao S, Zhai X, Li J, Xia A and Huang W, *Opt Express* **14**:810–816 (2006). https://doi.org/10.1364/OPEX.14.000810.
6 Maruo S, Ikuta K and Hayato K, Technical Digest. MEMS 2001. 14th IEEE International Conference on Micro Electro Mechanical Systems (Cat. No.01CH37090), pp. 594–597 (2001). https://doi.org/10.1109/MEMSYS.2001.906611
7 Danilevicius P, Rekstyte S, Balciunas E, Kraniauskas A, Jarasiene R, Sirmenis R *et al.*, *J Biomed Opt* **17**:081405 (2012). https://doi.org/10.1117/1.JBO.17.8.081405.
8 Marino A, Filippeschi C, Mattoli V, Mazzolai B and Ciofani G, *Nanoscale* **7**:2841–2850 (2015). https://doi.org/10.1039/c4nr06500j.
9 Xing J-F, Zheng M-L and Duan X-M, *Chem Soc Rev* **44**:5031–5039 (2015). https://doi.org/10.1039/c5cs00278h.
10 Kasko AM and Wong DY, *Future Med Chem* **2**:1669–1680 (2010). https://doi.org/10.4155/fmc.10.253.
11 Ovsianikov A, Malinauskas M, Schlie S, Chichkov B, Gittard S, Narayan R *et al.*, *Acta Biomater* **7**:967–974 (2011). https://doi.org/10.1016/j.actbio.2010.10.023.
12 Ovsianikov A, Schlie S, Ngezahayo A, Haverich A and Chichkov BN, *J Tissue Eng Regen Med* **1**:443–449 (2007). https://doi.org/10.1002/term.57.

13 Ovsianikov A, Deiwick A, Van Vlierberghe S, Dubruel P, Möller L, Drager G *et al.*, *Biomacromolecules* **12**:851–858 (2011). https://doi.org/10.1021/bm1015305.
14 Gittard SD, Ovsianikov A, Akar H, Chichkov B, Monteiro-Riviere NA, Stafslien S *et al.*, *Adv Eng Mater* **12**:B77–B82 (2010). https://doi.org/10.1002/adem.200980012.
15 Jia B, Buso D, Van Embden J, Li J and Gu M, *Adv Mater* **22**:2463–2467 (2010). https://doi.org/10.1002/adma.201000513.
16 Marino A, Barsotti J, De Vito G, Filippeschi C, Mazzolai B, Piazza V *et al.*, *ACS Appl Mater Interfaces* **7**:25574–25579 (2015). https://doi.org/10.1021/acsami.5b08764.
17 Ovsianikov A, Mühleder S, Torgersen J, Li Z, Qin XH, Van Vlierberghe S *et al.*, *Langmuir* **30**:3787–3794 (2014). https://doi.org/10.1021/la402346z.
18 Evans ND, Minelli C, Gentleman E, LaPointe V, Patankar SN, Kallivretaki M *et al.*, *Eur Cell Mater* **18**:1–13 (2009). https://doi.org/10.22203/eCM.v018a01.
19 Yin Z, Chen X, xin Song H, jie Hu J, mei Tang Q, Zhu T *et al.*, *Biomaterials* **44**:173–185 (2015). https://doi.org/10.1016/j.biomaterials.2014.12.027.
20 Hamid Q, Wang C, Snyder J and Sun W, *J Biomed Mater Res B* **103**:473–484 (2015). https://doi.org/10.1002/jbm.b.33223.
21 Thrivikraman G, Mallik PK and Basu B, *Biomaterials* **34**:7073–7085 (2013). https://doi.org/10.1016/j.biomaterials.2013.05.076.
22 Weiss T, Hildebrand G, Schade R and Liefeith K, *Eng Life Sci* **9**:384–390 (2009). https://doi.org/10.1002/elsc.200900002.
23 Basu S, Gomi K, Campagnola PJ, Kanazashi M, Lickorish D, Arai T *et al.*, *J Biomed Mater Res A* **71**:359–368 (2004). https://doi.org/10.1002/jbm.a.30174.
24 Mačiulaitis J, Deveikytė M, Rekštytė S, Bratchikov M, Darinskas A, Šimbelytė A *et al.*, *Biofabrication* **7**:015015 (2015). https://doi.org/10.1088/1758-5090/7/1/015015.
25 Nava MM, Piuma A, Figliuzzi M, Cattaneo I, Bonandrini B, Zandrini T *et al.*, *Stem Cell Res Ther* **7**:132 (2016). https://doi.org/10.1186/s13287-016-0387-z.
26 Farsari M, Vamvakaki M and Chichkov BN, *J Opt* **12**:124001 (2010). https://doi.org/10.1088/2040-8978/12/12/124001.
27 Nazir R, Bourquard F, Balčiūnas E, Smoleń S, Gray D, Tkachenko NV *et al.*, *ChemPhysChem* **16**:682–690 (2015). https://doi.org/10.1002/cphc.201402646.
28 Nazir R, Balčiunas E, Buczyńska D, Bourquard F, Kowalska D, Gray D *et al.*, *Macromolecules* **48**:2466–2472 (2015). https://doi.org/10.1021/acs.macromol.5b00336.
29 Nazir R, Thorsted B, Balčiunas E, Mazur L, Deperasińska I, Samoć M *et al.*, *J Mater Chem C* **4**:167–177 (2015). https://doi.org/10.1039/c5tc03334a.
30 Nazir R, Danilevicius P, Gray D, Farsari M and Gryko DT, *Macromolecules* **46**:7239–7244 (2013). https://doi.org/10.1021/ma4010988.
31 Nazir R, Danilevicius P, Ciuciu AI, Chatzinikolaidou M, Gray D, Flamigni L *et al.*, *Chem Mater* **26**:3175–3184 (2014). https://doi.org/10.1021/cm500612w.
32 Malinauskas M, Gaidukevičiute A, Purlys V, Žukauskas A, Sakellari I, Kabouraki E *et al.*, *Metamaterials* **5**:135–140 (2011). https://doi.org/10.1016/j.metmat.2011.04.002.
33 Sakellari I, Gaidukeviciute A, Giakoumaki A, Gray D, Fotakis C, Farsari M *et al.*, *Appl Phys A* **100**:359–364 (2010). https://doi.org/10.1007/s00339-010-5864-0.
34 Kabouraki E, Giakoumaki AN, Danilevicius P, Gray D, Vamvakaki M and Farsari M, *Nano Lett* **13**:3831–3835 (2013). https://doi.org/10.1021/nl401853k.
35 Ovsianikov A, Viertl J, Chichkov B, Oubaha M, MacCraith B, Sakellari I *et al.*, *ACS Nano* **2**:2257–2262 (2008). https://doi.org/10.1021/nn800451w.
36 Malinauskas M, Žukauskas A, Purlys V, Belazaras K, Momot A, Paipulas D *et al.*, *J Opt* **12**:124010 (2010). https://doi.org/10.1088/2040-8978/12/12/124010.
37 Vasilantonakis N, Terzaki K, Sakellari I, Purlys V, Gray D, Soukoulis CM *et al.*, *Adv Mater* **24**:1101–1105 (2012). https://doi.org/10.1002/adma.201104778.
38 Raimondi MT, Eaton SM, Laganà M, Aprile V, Nava MM, Cerullo G *et al.*, *Acta Biomater* **9**:4579–4584 (2013). https://doi.org/10.1016/j.actbio.2012.08.022.
39 Rezende RA, Pereira FDAS, Kasyanov V, Ovsianikov A, Torgensen J, Gruber P *et al.*, *Virtual Phys Prototyping* **7**:287–301 (2012). https://doi.org/10.1080/17452759.2012.740877.
40 Nava MM, Di Maggio N, Zandrini T, Cerullo G, Osellame R, Martin I *et al.*, *J Tissue Eng Regen Med* **11**:2836–2845 (2016). https://doi.org/10.1002/term.2187.
41 Ovsianikov A, Shizhou X, Farsari M, Vamvakaki M, Fotakis C and Chichkov BN, *Opt Express* **17**:2143–2148 (2009). https://doi.org/10.1364/OE.17.002143.
42 Terzaki K, Kissamitaki M, Skarmoutsou A, Fotakis C, Charitidis CA, Farsari M *et al.*, *J Biomed Mater Res A* **101**:2283–2294 (2013). https://doi.org/10.1002/jbm.a.34516.
43 Malinauskas M, Baltriukiene D, Kraniauskas A, Danilevicius P, Jarasiene R, Sirmenis R *et al.*, *Appl Phys A* **108**:751–759 (2012). https://doi.org/10.1007/s00339-012-6965-8.
44 Psycharakis S, Tosca A, Melissinaki V, Giakoumaki A and Ranella A, *Biomed Mater* **6**:045008 (2011). https://doi.org/10.1088/1748-6041/6/4/045008.
45 Poinern GEJ, Le XT, O'Dea M, Becker T and Fawcett D, *Biomed Res Int* **2014**:238762 (2014). https://doi.org/10.1155/2014/238762.
46 Kolekar TV, Thorat ND, Yadav HM, Magalad VT, Shinde MA, Bandgar SS *et al.*, *Ceram Int* **42**:5304–5311 (2016). https://doi.org/10.1016/j.ceramint.2015.12.060.
47 Käpylä E, Sorkio A, Teymouri S, Lahtonen K, Vuori L, Valden M *et al.*, *Langmuir* **30**:14555–14565 (2014). https://doi.org/10.1021/la5023642.
48 Claeyssens F, Hasan EA, Gaidukeviciute A, Achilleos DS, Ranella A, Reinhardt C *et al.*, *Langmuir* **25**:3219–3223 (2009). https://doi.org/10.1021/la803803m.
49 Mercille S and Massie B, *Biotechnol Bioeng* **44**:1140–1154 (1994). https://doi.org/10.1002/bit.260440916.
50 Eisenbarth E, Velten D, Müller M, Thull R and Breme J, *Biomaterials* **25**:5705–5713 (2004). https://doi.org/10.1016/j.biomaterials.2004.01.021.
51 Elbert DL and Hubbell JA, *Annu Rev Mater Sci* **26**:365–394 (1996). https://doi.org/10.1146/annurev.ms.26.080196.002053.
52 Liu X, Chen S, Tsoi JKH and Matinlinna JP, *Regen Biomater* **4**:315–323 (2017). https://doi.org/10.1093/rb/rbx027.
53 Geetha M, Singh AK, Asokamani R and Gogia AK, *Prog Mater Sci* **54**:397–425 (2009). https://doi.org/10.1016/j.pmatsci.2008.06.004.
54 Hisbergues M, Vendeville S and Vendeville P, *J Biomed Mater Res B* **88**:519–529 (2009). https://doi.org/10.1002/jbm.b.31147.
55 Zeng Y, Yan Y, Yan H, Liu C, Li P, Dong P *et al.*, *J Mater Sci* **53**:6291–6301 (2018). https://doi.org/10.1007/s10853-018-1992-2.
56 Chen X, Chen C, Zhang H, Huang Y, Yang J and Sun D, *Carbohydr Polym* **173**:547–555 (2017). https://doi.org/10.1016/j.carbpol.2017.06.036.
57 Bondy SC, *Neurotoxicology* **31**:575–581 (2010). https://doi.org/10.1016/j.neuro.2010.05.009.
58 Abdel-Hady Gepreel M and Niinomi M, *J Mech Behav Biomed Mater* **20**:407–415 (2013). https://doi.org/10.1016/j.jmbbm.2012.11.014.
59 Krewski D, Yokel RA, Nieboer E, Borchelt D, Cohen J, Harry J *et al.*, *J Toxicol Environ Health B* **10**:1–269 (2007). https://doi.org/10.1080/10937400701597766.

